



GPR-derived ice thickness of the temperate Hintereisferner glacier (Austrian Alps): evaluation of thickness models

Lelde Švinka¹, Kristaps Lamsters¹, Jānis Karušs¹, Pēteris Džeriņš¹, Jurijs Ješkins¹

¹Faculty of Science and Technology, University of Latvia, Jelgavas Street 1, LV-1004, Riga, Latvia

5 *Correspondence to:* Lelde Švinka (lelde.svinka@lu.lv)

Abstract. Alpine glaciers are retreating rapidly and have a potential for near complete ice loss at the end of the 21st century thus accurate glacier evolution models are crucial for predicting the magnitude and rate of future glacier changes. Without reliable ice thickness assessments, such models lack credibility and cannot be validated, thus here we evaluate several ice thickness models and present new ground-penetrating radar (GPR) ice-thickness measurements of the Hintereisferner - a temperate glacier located in the Ötztal Alps, Austria, which despite of being one of the WGMS reference glaciers lacks up-to date measured ice thickness data.

The GPR data is characterized by strong signal scattering, typical for temperate ice with high water content, however the glacier bed is detectable in most profiles. GPR measurements reveal a maximum ice thickness of ~160 m along the central flowline and a mean thickness of ~81 m across the surveyed area. We further select three widely used, open-source ice-thickness models, GlabTop2, OGGM, and Millan et al. (2022), and compare their output to the GPR-derived ice thickness. All models systematically overestimate ice thickness across the surveyed area, with mean positive biases of ~37–40 m for GlabTop2 and OGGM and ~59 m for the Millan model, while only minor and localized underestimation occurs along the central flowline. These results highlight the limitations of predominantly geometry-based and velocity-informed modelling approaches when applied to small, temperate valley glaciers, where ice rheology and basal conditions may have greater influence on the resulting thickness than these algorithms allow.

The GPR data presented here is made freely available in the section “Code and data availability” and provides an updated ice thickness benchmark for the Hintereisferner, to be used for future model calibration and improvement for Alpine glacier evolution projections.

1 Introduction

25 Mountain glaciers have been retreating for the last few decades across the globe, and this rate has accelerated with each decade including alpine glaciers (Blunden and Arndt, 2020). Alpine glacier dynamics and their ongoing sensitivity to climate change are strongly influenced by glacier elevation, topography, and overall geometry (Fischer, 2010; Santin et al., 2019). While glacier inventories for the European Alps and Austria specifically are well developed (Fischer and Kuhn, 2013), direct



30 measurements of glacier thickness remain sparse in both space and time. Since ice thickness is a key parameter for estimating glacier volume and future evolution, this scarcity directly limits the accuracy of ice volume assessments and predictions.

To address this data gap, numerous modelling approaches have been developed to estimate glacier thickness and volume, mainly by utilizing information about glacier surface characteristics such as shape, slope, velocity or mass-balance, to invert for ice thickness. Further global or Alpine glacier evolution modelling (e.g Cook et al., 2023; Zekollari et al., 2024) relies on the accuracy of these ice thickness models. However, despite the broad applicability of thickness models, some studies have
35 shown that great discrepancies can arise between modelled and measured ice thickness at a local scale, particularly for relatively small valley glaciers, where simplifying assumptions and poorly constrained parameters can lead to large spatial and systematic errors (Forte et al., 2025; Lamsters et al., 2024; Švinka et al., 2025).

Thus, field-based studies remain vitally important, including datasets that are collected for prolonged periods, and can provide ice volume change estimates and help validate modelling results. As a notable case and an example is the Marmolada glacier
40 in the Dolomites, where repeated ground-penetrating radar (GPR) surveys conducted in 2004 and 2015 showed the reduction of the ice volume by ~30% and suggested possible glacier disappearance by mid-century (Santin et al., 2019). Alpine glacier retreat is accelerating as seen in numerous studies, for example, data from geodetic mass balance of glaciers in Ötztal Alps revealed that from 1969 to 2006 they experienced mean annual ice volume loss increase by ~50% and thickness reduction by more than ~70% (Abermann et al., 2009). More recent annual mass balance report of Swiss glaciers estimates the reduction of
45 the Swiss ice volume by 3.0% during the 2024/2025 hydrological year, and emphasize that “since 2015 one quarter of the Swiss glacier volume has been lost” (Huss et al., 2025). Even more - since 1973, more than 1,000 glaciers have completely vanished in the Swiss Alps (Linsbauer et al., 2025) highlighting the great sensitivity of such small Alpine glaciers. Projections suggest that this trend will continue, with up to two thirds of Alpine glacier volume lost by the end of the 21st century (vs. 2017) under RCP2.6 scenario and near-complete deglaciation under RCP8.5 (Hartl et al., 2025; Zekollari et al., 2019).

50 Hintereisferner (HEF), located in Rofental, Ötztal Alps, Austria, is one of the world reference glaciers of the World Glacier Monitoring Service (WGMS, 2024), and covered an area of 3.8 km² in 2023. It descends from 3.7 km a.s.l. to 2.5 km a.s.l. Long-term direct mass balance observations of HEF demonstrate that it has been losing mass since mid-20th century, with continuous negative balances since the mid-1980s and surface lowering of up to ~160 m at the glacier tongue by the early 2000s (Fischer, 2010; Fischer et al., 2012). Flow velocity, length, and thickness change observations at HEF span more than
55 150 years (Stocker-Waldhuber et al., 2024; Strasser et al., 2018), making it one of the best-documented Alpine glaciers. HEF is the key glaciological study site serving as an open-air laboratory and has been used as a test bed for various glaciological and meteorological applications (e.g. Mott et al., 2020; Strasser et al., 2018; Voordendag et al., 2023a, b). The long-time series of glaciological and meteorological observations have been also used to develop and validate glacier models (e.g. Maussion et al., 2019; Raper et al., 2000).

60 Despite this long research history, direct measurements of ice thickness remain limited. The most comprehensive GPR-based thickness dataset dates back to 2001 and consists of 145 point measurements, indicating a maximum ice thickness of 242 ± 13 m (Fischer and Kuhn, 2013). Subsequent GPR surveys have focused primarily on snow thickness rather than ice thickness



(Helfricht et al., 2014). As a result, no up-to-date, spatially detailed ice thickness dataset exists for HEF, limiting modelling and other studies which may benefit of ice thickness data for this reference glacier, including studies arising from the availability of a permanent long-range terrestrial laser scanning system since 2016 (Chambers et al., 2021; Voordendag et al., 2023b).

GPR is a widely used geophysical method for glacier thickness and internal structure investigations (Karušs et al., 2022, 2019; Lamsters et al., 2024; Navarro and Eisen, 2009; Sevestre et al., 2015; Lamsters et al., 2020a, b). The main factors influencing GPR performance in glacial environments include the specifications of a GPR system (e.g. frequency, power) and the physical properties of ice, such as density and water content, which affect dielectric permittivity and signal attenuation (Ogier et al., 2023; Schroeder et al., 2020; Watts and England, 1976). Temperate Alpine glaciers, including HEF, commonly contain liquid water, resulting in strong radar signal attenuation and limited bedrock detectability. As shown by Ogier et al. (2023), liquid water contents as low as ~0.2% (typical for Alpine glaciers) can significantly impede bed detection for ice thicknesses exceeding ~100 m.

In this study, we present new GPR-derived ice thickness measurements for HEF obtained using a low-frequency, hand-held radar system. Our objectives are to (1) provide an updated ice thickness dataset for this WGMS reference glacier, (2) assess the spatial variability of bedrock detectability under temperate conditions, and (3) evaluate the performance of commonly used ice thickness models against direct measurements.

2 Methods

The fieldwork on HEF in the Ötztal Alps was conducted in August 2023. Glacier thickness and internal structure data was gathered using GPR, while a GNSS receiver (Emlid Reach RS2) was used to ensure precise positioning of the GPR profiles (Fig. 1). A digital surface model (DSM) was obtained from an airborne laser scanning (ALS) campaign conducted on September 23, 2022, and provided by Rainer Prinz (Department of Atmospheric and Cryospheric Sciences, University of Innsbruck, Austria). The glacier outline was derived from Pléiades satellite images that were acquired on August 21, 2022 (Pléiades © CNES 2022, Distribution Airbus D&S).

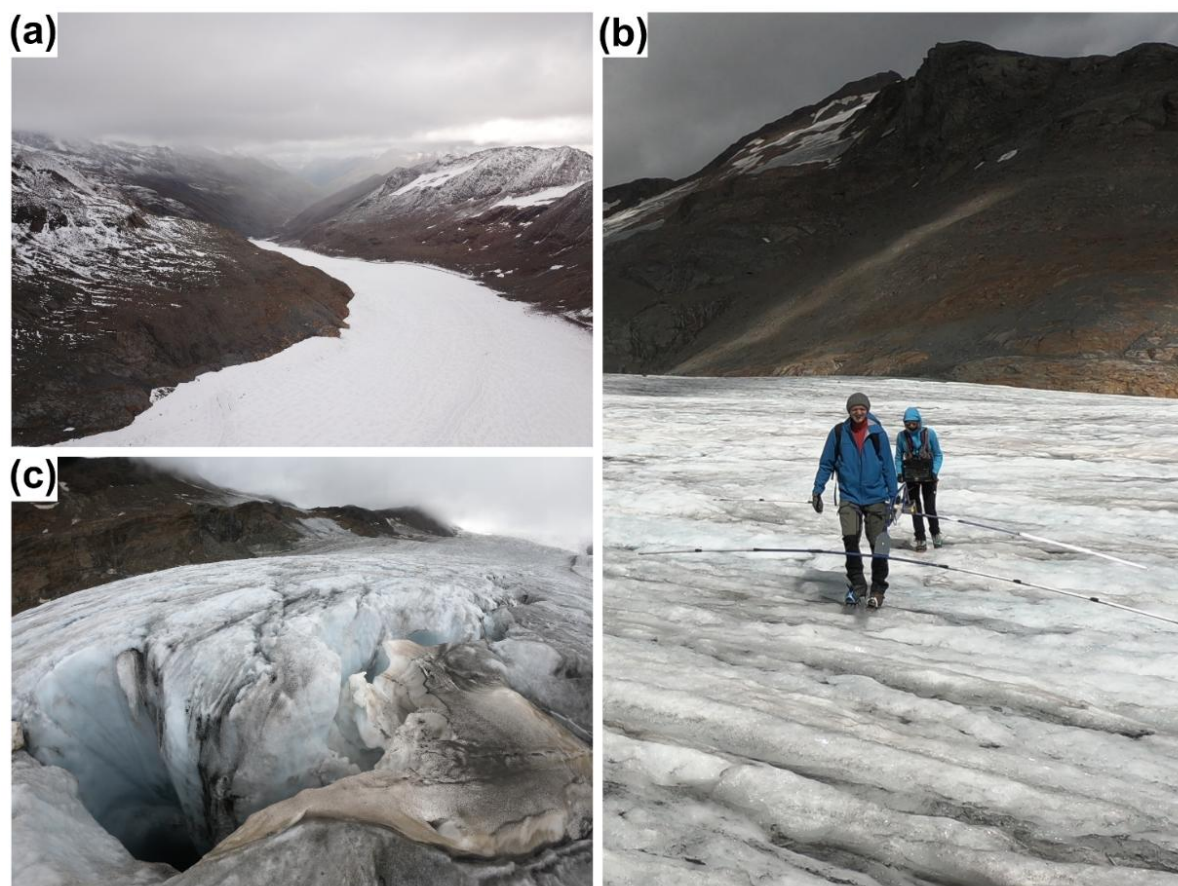


Figure 1: Photos from the field. (a) The surveyed area of the glacier. (b) GPR system and operator. (c) The largest moulin on a surface of the HEF in 2023.

2.1 GPR survey

90 In this study, we conducted a GPR survey using a hand-held Zond-xLF GPR system manufactured by Radar Systems, Inc. Given the temperate nature of Alpine glaciers, maximizing penetration depth was a priority, therefore, an antenna with the lowest possible frequency (38 MHz) compatible with our radar system was used, as higher-frequency signals are more susceptible to absorption in temperate ice conditions (Murray et al., 2007; Ogier et al., 2023). A time window of 2560 ns was selected, which allowed for a theoretical maximum penetration depth of ~210 m.

95 The GPR profiles were mainly oriented transverse to the ice flow direction with 200 m spacing in between to optimize data collection within the available timeframe and to gather enough data points for subglacial valley mapping. Additionally, one profile was recorded parallel to the ice flow direction (Fig. 2). Prior to the GPR survey, a waypoint plan with 50 m step size was created to ensure we could precisely and easily follow our predetermined profile layout on the glacier. During the survey, a Garmin Montana 610 GNSS receiver was used to navigate along the waypoints, while Emlid Reach RS2 GNSS receivers
100 provided precise positioning of the GPR profiles.

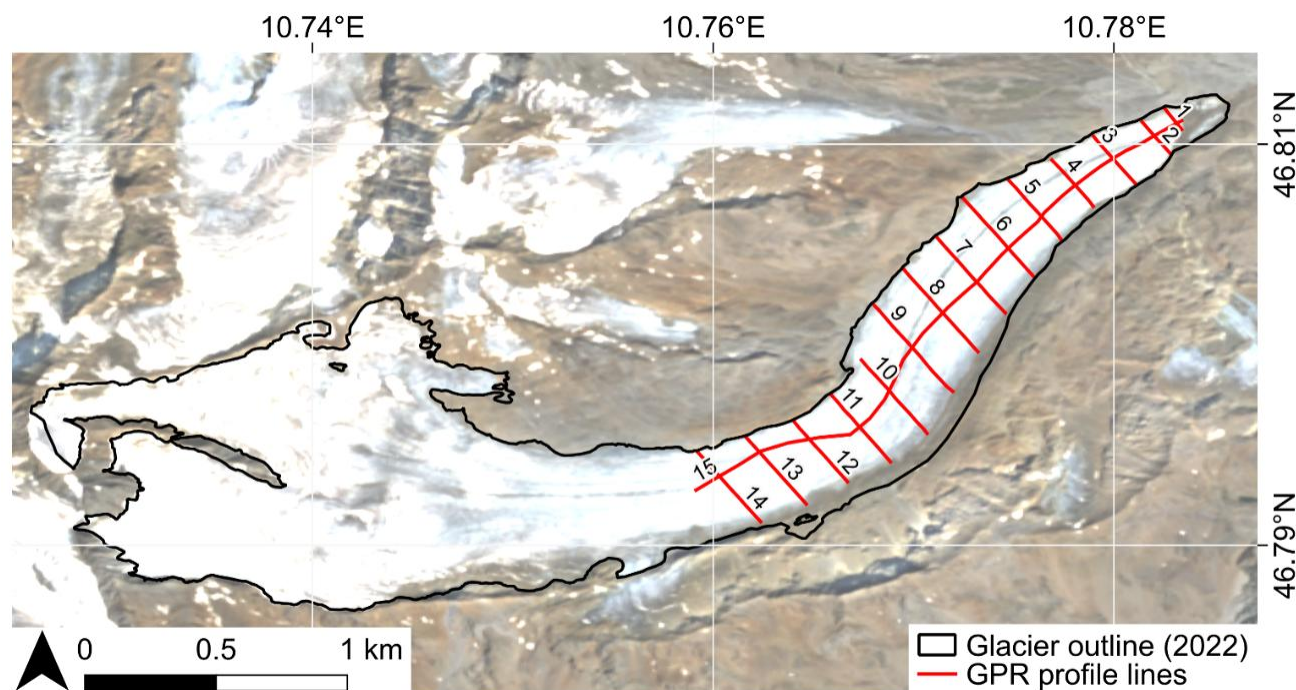


Figure 2: Hintereisferner glacier - profile location. Copernicus Sentinel-2 composite image (T32TPS_20230819T101609) at the background.

The gathered GPR data was processed using Prism 2.7 software. The processing workflow included the application of manually
 105 adjusted time-dependent signal gain function and Ormsby band-pass filter with a low frequency cut-off at 20 MHz and a high
 frequency cut-off at 70 MHz. Topographical corrections were applied using the elevation data from the DSM. During data
 interpretation, the two-way travel time (TWTT) for basal reflections was extracted from each B-scan along its entire length or
 where visible, with individual travel-time measurements picked approximately every 10 m. Due to intense internal signal
 scattering, a hyperbola matching function could not be applied for GPR signal velocity determination, and an equipment
 110 malfunction prevented us from conducting a common-midpoint survey. Consequently, the GPR propagation speed was set to
 0.168 m ns^{-1} , which corresponds to a dielectric permittivity of 3.2 - the typical value for cold ice conditions (Robin, 1975).
 The implications of this assumption are discussed in Sect. 2.3.

2.2 Thickness data and modelling

Glacier thickness point data derived from the GPR survey was interpolated using cubic interpolation algorithms. Cubic
 115 interpolation was chosen as a compromise between more simplistic methods (e.g. inverse-distance weighting) and more
 geostatistical approaches (e.g. kriging), providing a relatively smooth thickness field and honouring the measured values. To
 prevent unrealistic values along the glacier margins, a uniform boundary thickness of 0.1 m was assigned to points along the
 glacier outline. In addition to the GPR-derived ice thickness measurements, we evaluated three widely-used, open-source ice
 thickness models: GlabTop2 (Frey et al., 2014), OGGM v1.6.2. (Maussion et al., 2019), and Millan et al. (2022) global model.



120 These models differ in implementation algorithms and input data, although they ultimately derive ice thickness from glacier surface geometry and simplified ice flow assumptions.

The GlabTop2 model calculates ice thickness from surface slope using a shear-stress based approach, while the OGGM model inverts ice thickness along the central flowline based on mass conservation laws, constrained by the geodetic mass balance data. The Millan et al. (2022) in their model invert ice thickness from satellite-derived glacier surface velocities acquired in 125 years 2017-2018, utilizing regionally calibrated ice rheology parameters and geometry-based regularization.

For the GlabTop2 and OGGM models, we used open-source Python implementations with glacier outline and digital elevation model (DEM) as input, while for the Millan et al. (2022) ice thickness was extracted directly from the published dataset. However, since Millan et al. (2022) dataset represents glacier conditions for the 2017-2018 period, for the accuracy assessment, the thickness values were adjusted to account for the temporal offset to our GPR data acquisition date of August 2023. The 130 cumulative specific mass balance of -9.8 m w.e. was recorded for 2018-2023 (WGMS, 2024), which is equivalent to -10.9 m of ice thinning, assuming an ice density of 900 kg m^{-3} . This correction was applied only for the statistical comparison, while all visual materials (maps, difference maps, and scatterplot) retain the original 2017-2018 geometry.

All scripts used for model setup and execution are provided in the Supplement to ensure full reproducibility. All generated maps are in WGS84/UTM zone 32N coordinate system and ellipsoidal height.

135 2.3 Uncertainty and accuracy assessment

All uncertainty and accuracy calculations were made on the measured GPR point data ($n = 1313$), while the interpolated thickness and bedrock maps were used solely for visualization purposes to avoid introducing interpolation artefacts.

In our survey GPR velocity could not be measured *in-situ*, therefore a standard cold-ice (0% water content) velocity value of 0.168 m ns^{-1} was applied, introducing a systematic bias in our GPR-derived thickness values. Given that Hintereisferner is 140 classified as a temperate glacier and some level of internal scattering is visible in all the B-scans, possibly indicating high water saturation, the true EM velocity likely is lower, as it decreases with increasing liquid-water content (Navarro and Eisen, 2009). This would result in shallower true ice thickness than calculated using the cold-ice value of 0.168 m ns^{-1} .

Following the survey of the temperate Falljökull glacier in Iceland by Murray et al. (2000), where a mean EM velocity of 0.156 m ns^{-1} was measured, our assumed value would correspond to +7% systematic overestimation in ice thickness. In 145 addition, uncertainty in the resolution of bed-reflection picking introduces a locally variable random error of $\lambda/2$, which for our 38 MHz antenna and EM velocity of 0.168 m ns^{-1} equals 2.2 m (~2-3% of the mean ice thickness). Considering both sources of uncertainty - the dominant positive velocity bias and the smaller, spatially variable picking error - the worst-case overestimation of ice thickness is likely up to ~10%, whereas the typical uncertainty represents a positive bias of only a few percent.

150 To evaluate the accuracy of modelled ice thickness data, we compared the modelled and measured (GPR-derived) values using mean error or bias (ME), relative error (RE), and root-mean-square error (RMSE), defined as:



$$ME = \frac{1}{n} \sum_{i=1}^n (h_{mod,i} - h_{GPR,i}), \quad (1)$$

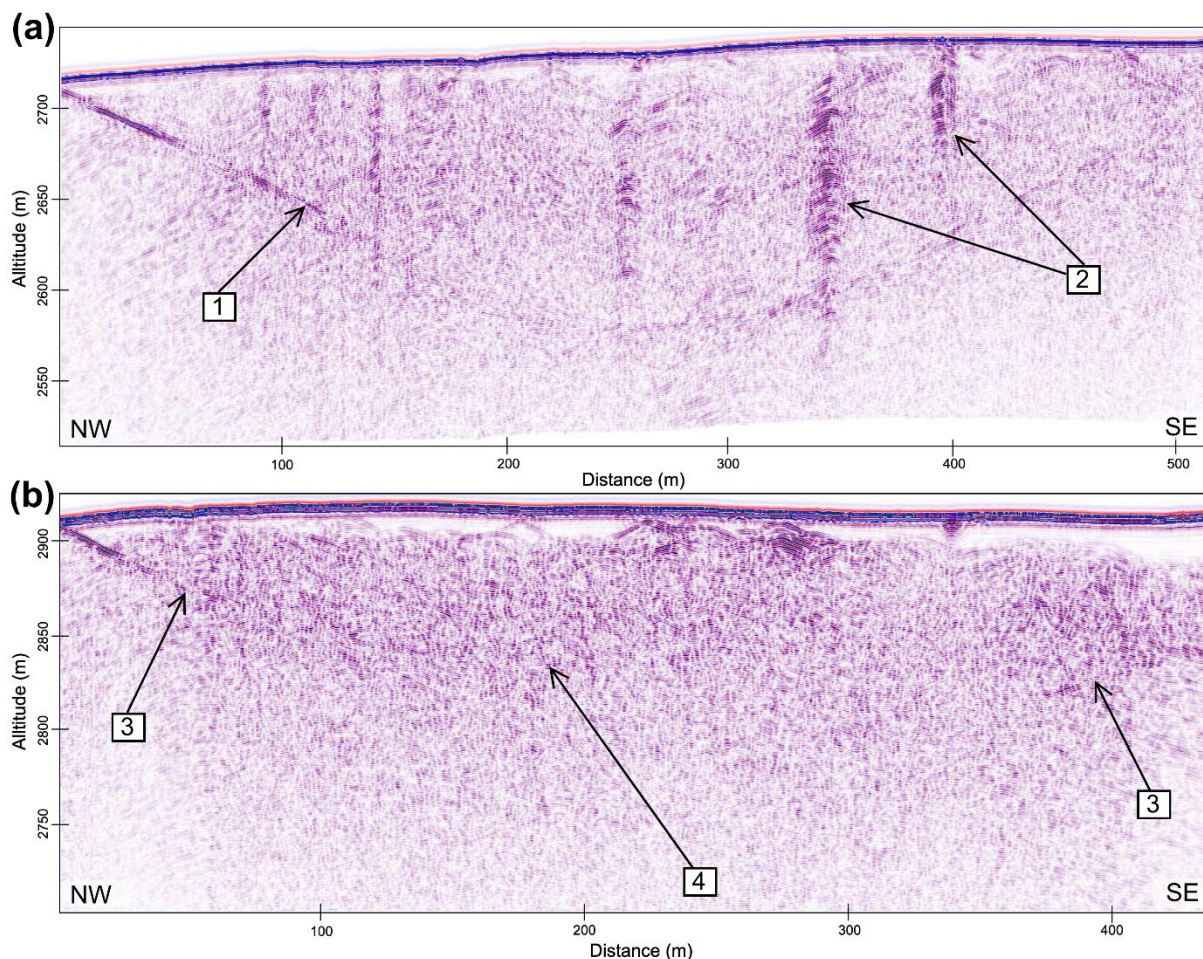
$$RE = \frac{h_{mod} - h_{GPR}}{h_{GPR}} \cdot 100\%, \quad (2)$$

$$RMSE = \sqrt{\frac{1}{n} \sum_{i=1}^n (h_{mod,i} - h_{GPR,i})^2}, \quad (3)$$

155 where h_{mod} and h_{GPR} are the modelled and measured ice thickness, respectively. These metrics were chosen to summarize the direction and magnitude of deviation from the GPR measurements in a simple and interpretable way.

3 Results

During fieldwork, 15 B-scans were collected, spanning approximately 8.5 km and covering ~ 1.3 km² of the HEF. GPR signal quality varied spatially, with strong and well-defined basal reflections (Fig. 3a) in the lower ablation area (Fig. 2, profiles 1-8) and increasingly obscured reflections (Fig. 3b) towards higher elevations along the centre flowline (Fig. 2, profiles 9-15).
160 Notably, in the B-scan recorded along the ice flow direction (Fig. 2, profile 15), the glacier bed was obscured in several sections where it was visible in the transverse profiles. Except for reflections from the glacier bed and vertically stacked hyperbolae attributed to supraglacial channels and crevasses, B-scans are characterized by intense EM wave scattering (Fig. 3). Such scattering according to numerous studies of polythermal and temperate glaciers in Svalbard (Karušs et al., 2022; Sevestre et al., 2015), Iceland (Lamsters et al., 2020b; Murray et al., 2000), Sweden (Gusmeroli et al., 2012; Rippin et al., 2011), Greenland (Forte et al., 2025; Lamsters et al., 2024) and Alps (Binder et al., 2009; Rutishauser et al., 2015; Santin et al., 2019) is clearly an indication of temperate ice with high water content. There is basically no transparent (scatter-free) ice except for very topmost part of few profiles at the highest elevation (Fig. 3b) that may be related to a piezometric surface, above which the water content decreases sharply (Murray et al., 2000; Lamsters et al., 2000b).
165



170

Figure 3: Examples of GPR profiles. (a) Profile 6 and (b) Profile 13 (see Fig.1 for locations). Numbers indicate: 1 - clearly visible glacier bed; 2 - reflections from supraglacial channels and crevasses; 3 - partially visible glacier bed; 4 - zone of intense signal scattering.

3.1 Subglacial topography and ice thickness

175

The interpolated ice thickness map (Fig. 4c) reveals a distinct subglacial trough aligned with the glacier flow. The maximum detected ice thickness of ~160 m occurs along the central flowline at an elevation of ~2870 m, while ice gradually thins toward both the margins and the terminus. The mean ice thickness of the surveyed area is ~81 m. The derived bedrock topography (Fig. 4d) reveals a U-shaped valley with bedrock elevations ranging from ~2540 to 2940 m. The longitudinal glacier cross-section (Fig. 4d, inset) indicates a down-glacier gradient with an evident rise in bedrock topography at around 1.8 km from the terminus.

180

This coincides with an apparent local thinning in the interpolated thickness map (Fig. 4c) and a steeper slope visible in the DSM (Fig. 4a). However, the glacier bed is not fully identifiable in the GPR profiles at this location (Fig. 4b), therefore the apparent thinning might also be an artefact from the lack of bedrock measurements. Overall, the spatial pattern of interpolated thickness and derived bedrock topography is best represented in the lower half of the survey area, where bed



visibility was highest, and the uncertainty increases toward the upper half of the survey area, where interpolation relied on
 185 fewer measurement points.

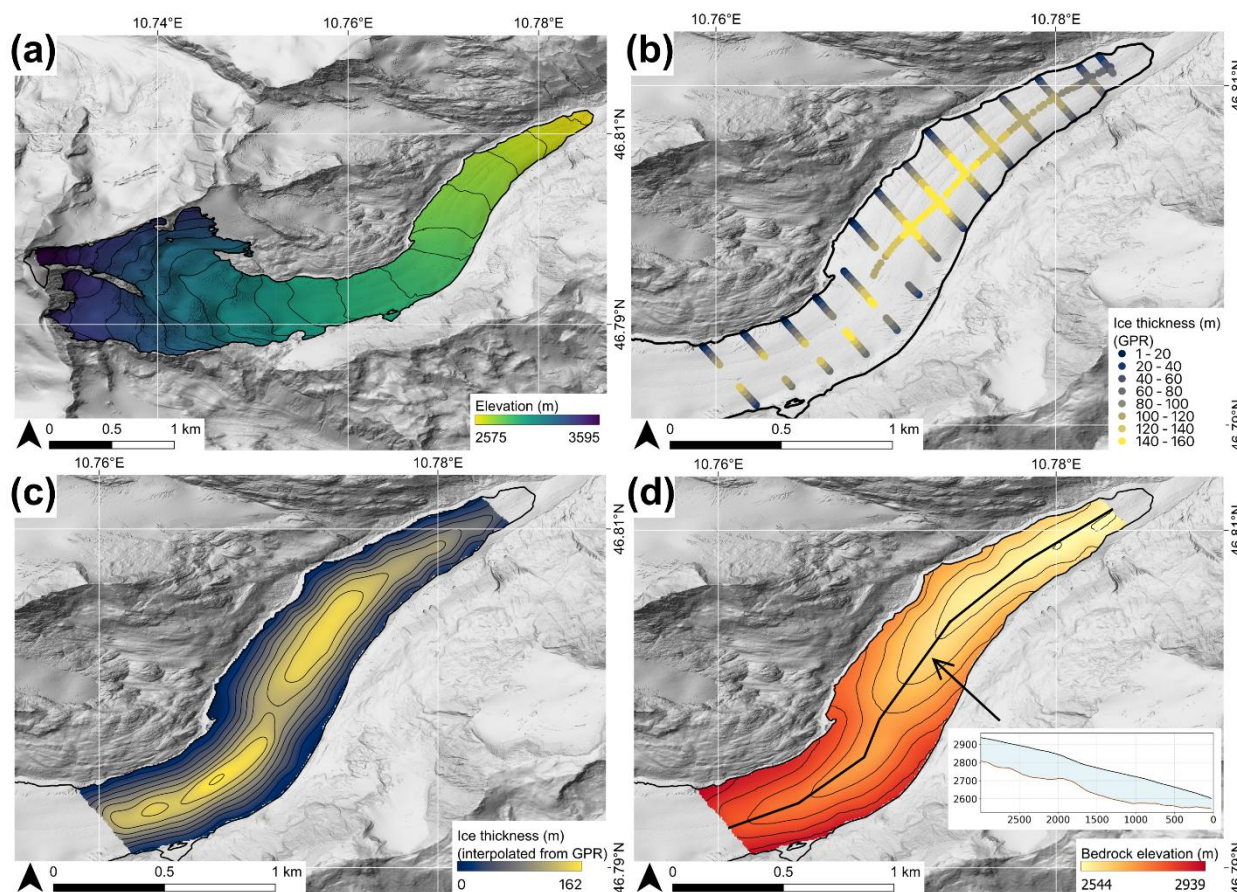


Figure 4: (a) Surface elevation from the 2022 DSM (contour interval 50 m). (b) Measured GPR ice thickness points. (c) Interpolated ice thickness distribution (contour interval 20 m). (d) Bedrock elevation (contour interval 50 m) derived from interpolated GPR data with longitudinal profile along the central flowline (inset). Background hillshaded DEM data source: basemap.at (basemap.at, 2024).

190 **3.2 Ice thickness models**

The modelled ice thickness distributions from GlabTop2, OGGM and Millan et al. (2022) represent the entire glaciated area, while the comparison with GPR data is limited to the GPR-surveyed region. All three models generally reproduce similar geometries, with maximum thickness in the lower half of the glacier - coinciding with the GPR-surveyed area - and thinner towards higher elevations and steeper slopes (Fig. 5a, c, e). The maximum modelled ice thickness is 157 m for GlabTop2, 226
 195 m for OGGM, and 247 m for Millan et al. (2022).

The thickness difference maps between modelled and GPR-derived (interpolated) thickness (Fig. 5b, d, f) reveal a consistent pattern of overestimation, particularly along the glacier margins. Maximum positive deviations range from ~150 m (GlabTop2 and OGGM) to 216 m (Millan et al. 2022), while negative deviations are comparatively small, reaching -13 m for OGGM, -



36 m for GlabTop2, and -67 m for Millan et al. (2022). Ice thickness tends to be slightly underestimated along the centre
200 flowline for the GlabTop2 and Millan models, although these values are an order of magnitude smaller than the overestimations.

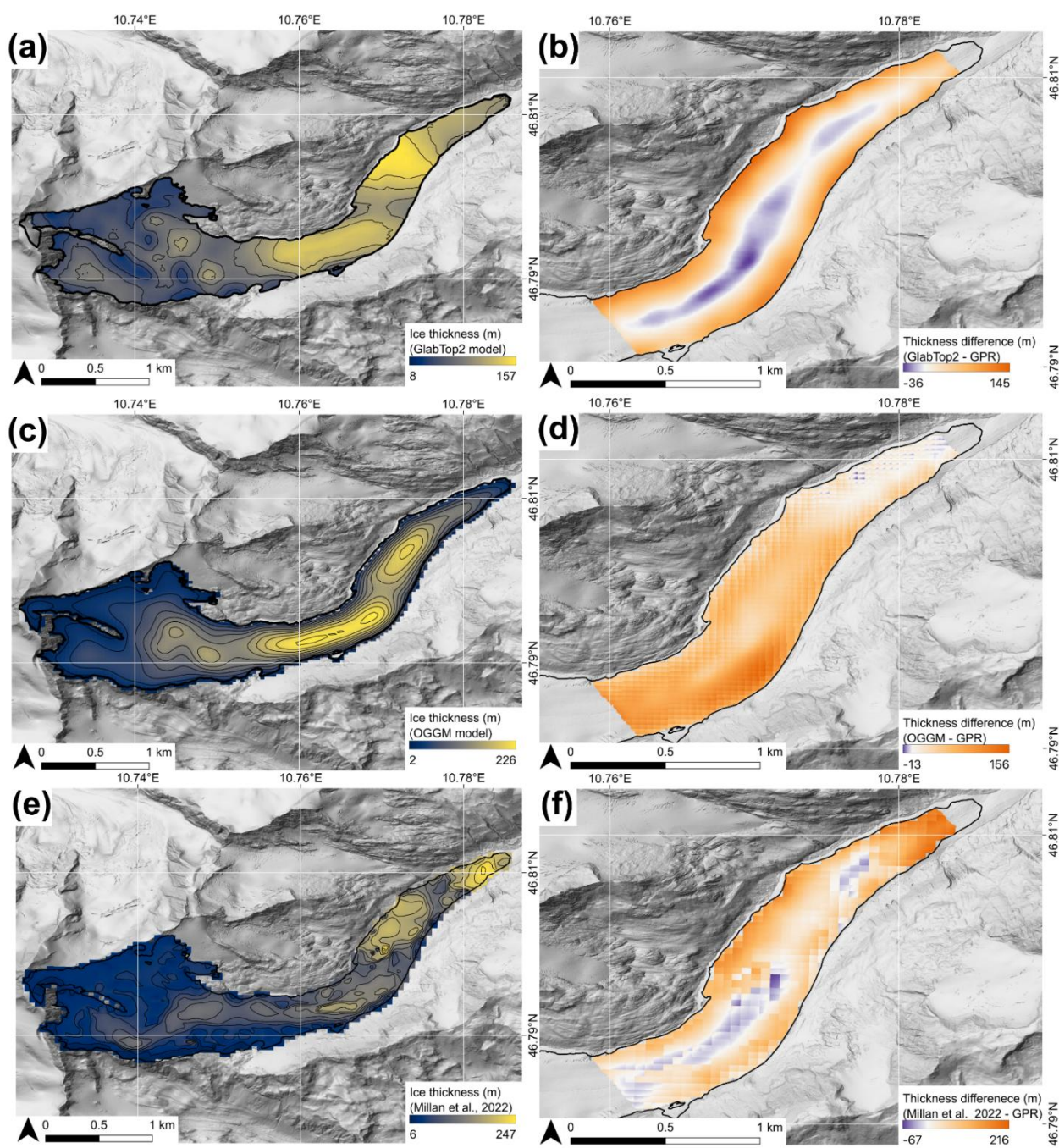


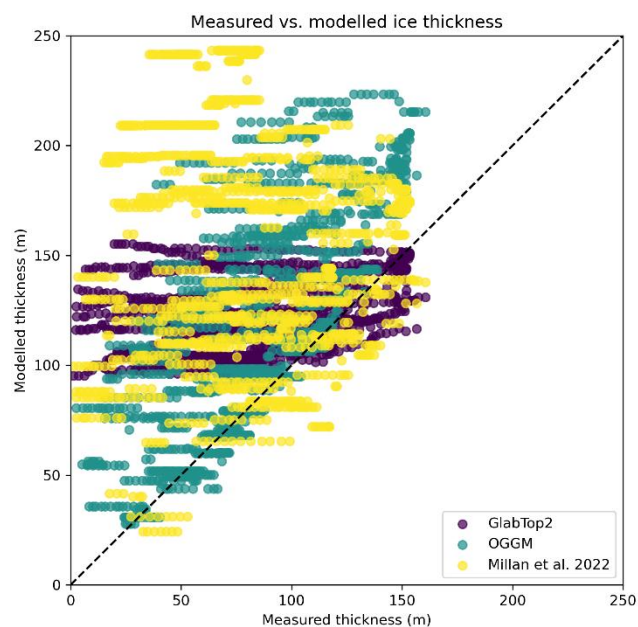
Figure 5: Thickness models (contour interval 20 m) and difference between a model and GPR derived interpolated ice thickness. Background hillshaded DEM data source: basemap.at (basemap.at, 2024).



205

The mean modelled ice thickness ranges from ~120 m (GlabTop2 and OGGM) to ~140 m Millan et al. (2022) model after adjusting for the cumulative mass loss between 2018 and 2023 (Table 1). The corresponding mean errors are +40 m for GlabTop2, +37 m for OGGM, and +59 m for Millan model, with RMSE of 54, 51 and 92 m, respectively. These results reveal a consistent positive bias across all three models, reflecting a general pattern of ice thickness overestimation, also visible in measured vs. modelled data scatterplot (Fig. 6). Here GlabTop2 data show a relatively narrow range of ice thickness, mostly between 100 and 150 m, indicating that model tends to produce spatially uniform distribution and fails to represent the local extremes, as revealed by the GPR data. In contrast, the OGGM and Millan et al. (2022) models show a wider spread of modelled values, reproducing both thicker and thinner sections more realistically, however still severely overestimating the overall ice thickness across the survey area.

210



215

Figure 6: Comparison between measured and modelled ice thickness across the GPR-surveyed area.

Table 1: Statistical comparison between GPR-derived and modelled ice thickness values.

$n = 1313$	\bar{h} (m)	$RE_{\bar{h}}$ (%)	ME (m)	$RMSE$ (m)
GPR	81.1	-	-	-
GlabTop2	121.1	49.4	40.1	54.1
OGGM	120.4	48.5	37.4	50.8



Millan et al. 2022 (adjusted)	139.8	72.5	58.6	91.6
-------------------------------------	-------	------	------	------

4 Discussion

4.1 Ice thickness model performance and influencing factors

- 220 The comparison between GPR-derived ice thickness and the three modelling approaches used in this study reveals a systematic ice thickness overestimation across the surveyed area of HEF, however its magnitude is comparable for GlabTop2 and OGGM models, while the Millan et al. (2022) model produces substantially larger errors. Differences between GlabTop2 and OGGM lie primarily in the spatial distribution of the ice thickness. The OGGM model does not exhibit ice thickness underestimation along the central flowline in this case, likely reflecting the valley-confined geometry of HEF, for which the flowline-based
- 225 algorithm and enforced flux continuity of this model are particularly well suited (Maussion et al., 2019). On the other hand, the locally slope-controlled GlabTop2 algorithm produces a more homogeneous thickness field and locally underestimates thickness in the central part of the glacier. Similar sensitivities of GlabTop2 model to slope and DEM quality, and the relative robustness of OGGM to these factors, have been documented in other model intercomparison studies (Chen et al., 2022; Pelto et al., 2020).
- 230 Despite using observed surface velocities in thickness inversion algorithm, the Millan et al. (2022) model produces the largest bias. Millan et al. report an accuracy of $\sim 10 \text{ m yr}^{-1}$ for their satellite-derived velocity mosaics, which are provided on a 50 m grid. For HEF, however, surface velocities during the past decade are generally below $\sim 10 \text{ m yr}^{-1}$ (Stocker-Waldhuber et al., 2024), with only localized areas possibly reaching higher values. As a result, the velocity signal is close to the uncertainty level of the velocity mosaic and provides only weak constraint on ice thickness magnitude. Under these conditions, ice
- 235 thickness becomes the primary variable used to satisfy the flux continuity, leading to systematic overestimation in this case. Although the three models differ in complexity and input data, they remain fundamentally constrained by glacier surface geometry and slope-dependent stress balance assumptions. In the absence of glacier-specific constraints on basal sliding and ice rheology, variations in ice viscosity must be balanced by the inferred thickness. Deviations from commonly assumed rheological parameters, such as a Glens' stress exponent n and rate factor A expected for temperate, water-rich ice, would
- 240 reduce the thickness required to reproduce the observed velocities. Recent studies show that temperate ice may behave substantially differently from cold ice, with the stress exponents approaching $n \approx 1$ (Schohn et al., 2025) and strong weakening associated with meltwater content and strain localization (Haseloff et al., 2019). If these effects are not accounted for, deformation-based inversions tend to misattribute ice motion to increased thickness, resulting in systematic overestimation. Although local underestimation occurs in places, the net effect across the surveyed area is a positive bias.
- 245 The contrasting behaviour of the Millan et al. (2022) model across different glaciological settings further highlights this sensitivity. While the model overestimates thickness for the temperate, valley-confined HEF, Lamsters et al. (2024) reported



substantial underestimation of up to ~80–90 m along the central flowline for small, narrow, cold outlet glaciers of the Qaanaaq Ice Cap in NW Greenland. These opposite biases likely reflect the same inversion process acting under different thermal and velocity conditions, showing that velocity-based approaches depend strongly on glacier size, geometry, and ice rheology.

250 Finally, the spatial extent of GPR survey in this study must be considered when interpreting model performance. The comparison is restricted to the middle-to-lower sections of HEF, where surface slopes are relatively gentle. The steeper upper-glacier area and potential local thickness maxima were not fully covered, and bed visibility decreased towards higher elevations. Inclusion of these areas could potentially reduce the overall magnitude of overestimation, but no definitive conclusions can be drawn. In addition, our use of a constant EM wave velocity representative of cold ice likely leads to a slight

255 underestimation of true thickness in temperate ice (see Sect. 2.3), but the magnitude of this underestimation would not alter the overall positive bias of the models within our survey area, which on average still substantially overestimate ice thickness.

4.2 Implications for GPR surveys on temperate glaciers

Ground-based GPR systems are generally considered to provide the highest data quality and bedrock detection capability in temperate Alpine glaciers (Forte et al., 2019; Rutishauser et al., 2015). Nevertheless, our results confirm other authors

260 conclusions that even ground-based systems can suffer from low bedrock visibility in temperate ice (Vergano et al., 2025) particularly where thickness exceeds ~100 m (Binder et al., 2009). Although winter surveys are sometimes used to reduce attenuation from liquid water and improve bedrock detectability, such conditions pose substantial logistical and safety challenges for ground-based GPR on Alpine glaciers due to deep snow cover and limited accessibility. In such cases, combined interpretation of GPR measurements and modelled thickness has been recommended to reduce uncertainty (Vergano et al.,

265 2025); however, the pronounced model biases identified in this study indicate that such approaches must be applied with caution and cannot be universally recommended.

At HEF, highly crevassed and steep upper glacier section limited access with our ground-based system, therefore helicopter-borne GPR may be the only viable option for complete spatial coverage. While airborne surveys offer substantially larger coverage (e.g. Grab et al., 2021), they also involve trade-offs in resolution and signal penetration, particularly in temperate ice

270 (Forte et al., 2019). Drone-based GPR systems show growing potential for shallow and snow-covered glaciers (Ruols et al., 2025; Tjoelker et al., 2024) but remain largely unsuitable for reliable bedrock detection beneath thick temperate ice, with only few successful surveys to date (Ruols et al., 2023).

In addition, our GPR data reveal pronounced variations in basal reflection strength between profiles acquired parallel and perpendicular to ice flow. Similar directional effects have been reported previously (Moran et al., 2003; Nobes, 1999; Nobes and Annan, 2000) and attributed mainly to bedrock geometry (Langhammer et al., 2017). However, at HEF, we also observe

275 strong reflection variability between profiles with similar antenna orientation and without apparent bedrock changes, suggesting that spatial variations in temperate ice properties, such as water content, grain orientation, or crevassing, may play a more important role in radar attenuation than previously assumed.



5 Conclusions

280 The Hintereisferner glacier is one of the WGMS reference glaciers in the Ötztal Alps (Austria), with a long history of
glaciological observations, yet lacking up-to-date ice thickness data. To address this gap, we carried out detailed low-frequency
GPR measurements in August 2023 covering ~8.5 km of profiles and ~1.3 km² of the glacier surface. Despite strong signal
attenuation typical for temperate Alpine glaciers, the glacier bed was identifiable in most profiles; however, bed visibility
locally decreased in areas of strong signal scattering and showed sensitivity to radar antenna orientation. The maximum
285 detected ice thickness reaches ~160 m along the central flowline, while the mean thickness across the surveyed area is ~81 m.
The derived bedrock topography reveals a well-defined U-shaped valley, consistent with the glacier geometry.
We also compared three widely applied ice thickness models (GlabTop2, OGGM and Millan et al., 2022) to our GPR data and
found that the ice thickness in models is generally overestimated across the surveyed area. The mean modelled thickness range
from ~120 m (GlabTop2 and OGGM) to ~140 m (Millan et al., 2022, adjusted for 2023), corresponding to mean errors of
290 +37–40 m for GlabTop2 and OGGM and +59 m for the Millan model. Our results highlight persistent limitations of both
geometry-based and velocity-informed models when applied to small, temperate valley glaciers, where ice rheology and basal
conditions are difficult to constrain. These findings underscore the importance of continued field-based ice thickness
measurements for improving model calibration and reducing uncertainty in projections of temperate Alpine glacier change.
The dataset presented herein may additionally be used in improved future glacier evolution models.

295 Code and data availability

All the GPR data, derived bedrock picks, and model configuration and parameter files used in this study are available via a
Zenodo repository at: <https://doi.org/10.5281/zenodo.18542682> (Švinka et al., 2026). The repository is organized into four
subfolders, each accompanied by a README file, describing the contents and workflow steps.

A DSM was obtained from ALS campaign conducted on September 23, 2022, and provided by Rainer Prinz (Department of
300 Atmospheric and Cryospheric Sciences, University of Innsbruck, Austria). The glacier outline was derived from Pléiades
satellite images that were acquired on August 21, 2022 (Pléiades © CNES 2022, Distribution Airbus D&S).

Ice thickness modelling was performed using open-source models. The GlabTop2-Py model is available at [https://glabtop2-
py.readthedocs.io/en/latest/index.html](https://glabtop2-py.readthedocs.io/en/latest/index.html) (last access: 10 November 2025), and the OGGM model is available at
<https://docs.oggm.org/en/stable/> (last access: 10 November 2025). In addition, ice thickness estimates from the global ice
305 thickness model of Millan et al. (2022) were used. The thickness product was obtained from the THEIA data centre at
<https://www.sedoo.fr/theia-publication-products/?uuid=55acb5d5-3982-4eac-89b2-46703557938c> (last access: 10 November
2025).



Author contributions

Conceptualization: LŠ, KL, JK. Data Acquisition: LŠ, KL, PD. Data processing: LŠ, JJ. Data analyses: LŠ, KL, JK. Writing:
310 LŠ, KL, JK. Visualization: LŠ.

Competing interests

The authors declare that they have no conflict of interest.

Disclaimer

“Copernicus Publications remains neutral with regard to jurisdictional claims made in the text, published maps, institutional
315 affiliations, or any other geographical representation in this paper. While Copernicus Publications makes every effort to include
appropriate place names, the final responsibility lies with the authors. Views expressed in the text are those of the authors and
do not necessarily reflect the views of the publisher.”

Acknowledgements

Station Hintereis manager Rainer Prinz is warmly acknowledged for all logistical help and especially fast transportation to the
320 base via helicopter.

Financial support

The research leading to these results has received Transnational Access from the European Union’s Horizon 2020 project
INTERACT, under grant agreement No. 871120.

Review statement

325 The review statement will be added by Copernicus Publications listing the handling editor as well as all contributing referees
according to their status anonymous or identified.

References

Abermann, J., Lambrecht, A., Fischer, A., and Kuhn, M.: Quantifying changes and trends in glacier area and volume in the
Austrian Ötztal Alps (1969-1997-2006), *The Cryosphere*, 3, 205–215, <https://doi.org/10.5194/tc-3-205-2009>, 2009.
330 basemap.at: Geoland Basemap Gelände (hillshade) (last access: 10 November 2025), 2024.



- Binder, D., Brückl, E., Roch, K. H., Behm, M., Schöner, W., and Hynek, B.: Determination of total ice volume and ice-thickness distribution of two glaciers in the Hohe Tauern region, Eastern Alps, from GPR data, *Ann. Glaciol.*, 50, 71–79, <https://doi.org/10.3189/172756409789097522>, 2009.
- Blunden, J. and Arndt, D. S.: State of the Climate in 2019, *Bulletin of the American Meteorological Society*, 101, S1–S429, <https://doi.org/10.1175/2020BAMSStateoftheClimate.1>, 2020.
- 335 Chambers, J. R., Smith, M. W., Smith, T., Sailer, R., Quincey, D. J., Carrivick, J. L., Nicholson, L., Mertes, J., Stiperski, I., and James, M. R.: Correcting for Systematic Underestimation of Topographic Glacier Aerodynamic Roughness Values From Hintereisferner, Austria, *Front. Earth Sci.*, 9, 691195, <https://doi.org/10.3389/feart.2021.691195>, 2021.
- Chen, W., Yao, T., Zhang, G., Li, F., Zheng, G., Zhou, Y., and Xu, F.: Towards ice-thickness inversion: an evaluation of global digital elevation models (DEMs) in the glacierized Tibetan Plateau, *The Cryosphere*, 16, 197–218, <https://doi.org/10.5194/tc-16-197-2022>, 2022.
- 340 Cook, S. J., Jouvét, G., Millan, R., Rabatel, A., Zekollari, H., and Dussaillant, I.: Committed Ice Loss in the European Alps Until 2050 Using a Deep-Learning-Aided 3D Ice-Flow Model With Data Assimilation, *Geophysical Research Letters*, 50, e2023GL105029, <https://doi.org/10.1029/2023GL105029>, 2023.
- 345 Fischer, A.: Glaciers and climate change: Interpretation of 50 years of direct mass balance of Hintereisferner, *Global and Planetary Change*, 71, 13–26, <https://doi.org/10.1016/j.gloplacha.2009.11.014>, 2010.
- Fischer, A. and Kuhn, M.: Ground-penetrating radar measurements of 64 Austrian glaciers between 1995 and 2010, *Ann. Glaciol.*, 54, 179–188, <https://doi.org/10.3189/2013AoG64A108>, 2013.
- Fischer, A., Markl, G., and Kuhn, M.: Glacier Mass Balance of Hintereisferner, Oetztal Alps, Austria, from 1952/53–2010/11, https://doi.org/10.1594/WDCC/MB_HEF_1953-2011, 2012.
- 350 Forte, E., Bondini, M. B., Bortoletto, A., Dossi, M., and Colucci, R. R.: Pros and Cons in Helicopter-Borne GPR Data Acquisition on Rugged Mountainous Areas: Critical Analysis and Practical Guidelines, *Pure Appl. Geophys.*, 176, 4533–4554, <https://doi.org/10.1007/s00024-019-02196-2>, 2019.
- Forte, E., Gutgesell, P., Securo, A., Marcer, M., Citterio, M., Machguth, H., and Colucci, R. R.: Comparing GPR with ice thickness and thermal models: Insights from two polythermal glaciers in West Greenland, *J. Glaciol.*, 71, e97, <https://doi.org/10.1017/jog.2025.10067>, 2025.
- 355 Frey, H., Machguth, H., Huss, M., Huggel, C., Bajracharya, S., Bolch, T., Kulkarni, A., Linsbauer, A., Salzmann, N., and Stoffel, M.: Estimating the volume of glaciers in the Himalayan–Karakoram region using different methods, *The Cryosphere*, 8, 2313–2333, <https://doi.org/10.5194/tc-8-2313-2014>, 2014.
- 360 Grab, M., Mattea, E., Bauder, A., Huss, M., Rabenstein, L., Hodel, E., Linsbauer, A., Langhammer, L., Schmid, L., Church, G., Hellmann, S., Déléze, K., Schaer, P., Lathion, P., Farinotti, D., and Maurer, H.: Ice thickness distribution of all Swiss glaciers based on extended ground-penetrating radar data and glaciological modeling, *J. Glaciol.*, 67, 1074–1092, <https://doi.org/10.1017/jog.2021.55>, 2021.



- Gusmeroli, A., Jansson, P., Pettersson, R., and Murray, T.: Twenty years of cold surface layer thinning at Storglaciären, sub-
365 Arctic Sweden, 1989-2009, *J. Glaciol.*, 58, 3–10, <https://doi.org/10.3189/2012JoG11J018>, 2012.
- Hartl, L., Schmitt, P., Schuster, L., Helfricht, K., Abermann, J., and Maussion, F.: Recent observations and glacier modeling
point towards near-complete glacier loss in western Austria (Ötztal and Stubai mountain range) if 1.5 °C is not met, *The
Cryosphere*, 19, 1431–1452, <https://doi.org/10.5194/tc-19-1431-2025>, 2025.
- Haseloff, M., Hewitt, I. J., and Katz, R. F.: Englacial Pore Water Localizes Shear in Temperate Ice Stream Margins, *JGR Earth
370 Surface*, 124, 2521–2541, <https://doi.org/10.1029/2019JF005399>, 2019.
- Helfricht, K., Kuhn, M., Keuschnig, M., and Heilig, A.: Lidar snow cover studies on glaciers in the Ötztal Alps (Austria):
comparison with snow depths calculated from GPR measurements, *The Cryosphere*, 8, 41–57, <https://doi.org/10.5194/tc-8-41-2014>, 2014.
- Huss, M., Bauder, A., Linsbauer, A., and Barandun, M.: Annual mass balance of Swiss glaciers in 2024/2025, 2025.
- 375 Karušs, J., Lamsters, K., Chernov, A., Krievāns, M., and Ješkins, J.: Subglacial topography and thickness of ice caps on the
Argentine Islands, *Antarctic Science*, 31, 332–344, <https://doi.org/10.1017/S0954102019000452>, 2019.
- Karušs, J., Lamsters, K., Sobota, I., Ješkins, J., Džeriņš, P., and Hodson, A.: Drainage system and thermal structure of a High
Arctic polythermal glacier: Waldemarbreen, western Svalbard, *J. Glaciol.*, 68, 591–604, <https://doi.org/10.1017/jog.2021.125>,
2022.
- 380 Lamsters, K., Karušs, J., Krievāns, M., and Ješkins, J.: High-resolution orthophoto map and digital surface models of the
largest Argentine Islands (the Antarctic) from unmanned aerial vehicle photogrammetry, *Journal of Maps*, 16, 335–347,
<https://doi.org/10.1080/17445647.2020.1748130>, 2020a.
- Lamsters, K., Karušs, J., Krievāns, M., and Ješkins, J.: The thermal structure, subglacial topography and surface structures of
the NE outlet of Eyjabakkajökull, east Iceland, *Polar Science*, 26, 100566, <https://doi.org/10.1016/j.polar.2020.100566>, 2020b.
- 385 Lamsters, K., Karušs, J., Ješkins, J., Džeriņš, P., Ukai, S., and Sugiyama, S.: Geometry and thermal regime of the southern
outlet glaciers of Qaanaaq Ice Cap, NW Greenland, *Earth Surf Processes Landf.*, 49, 4275–4288,
<https://doi.org/10.1002/esp.5966>, 2024.
- Langhammer, L., Rabenstein, L., Bauder, A., and Maurer, H.: Ground-penetrating radar antenna orientation effects on
temperate mountain glaciers, *GEOPHYSICS*, 82, H15–H24, <https://doi.org/10.1190/geo2016-0341.1>, 2017.
- 390 Linsbauer, A., Huss, M., Hodel, E., Bauder, A., and Barandun, M.: Vanished glaciers of the Swiss Alps: An inventory-based
assessment from 1973 to 2016, *Ann. Glaciol.*, 66, e33, <https://doi.org/10.1017/aog.2025.10031>, 2025.
- Maussion, F., Butenko, A., Champollion, N., Dusch, M., Eis, J., Fourteau, K., Gregor, P., Jarosch, A. H., Landmann, J.,
Oesterle, F., Recinos, B., Rothenpieler, T., Vlug, A., Wild, C. T., and Marzeion, B.: The Open Global Glacier Model (OGGM)
v1.1, *Geosci. Model Dev.*, 12, 909–931, <https://doi.org/10.5194/gmd-12-909-2019>, 2019.
- 395 Millan, R., Mouginot, J., Rabatel, A., and Morlighem, M.: Ice velocity and thickness of the world’s glaciers, *Nat. Geosci.*, 15,
124–129, <https://doi.org/10.1038/s41561-021-00885-z>, 2022.



- Moran, M. L., Greenfield, R. J., and Arcone, S. A.: Modeling GPR radiation and reflection characteristics for a complex temperate glacier bed, *Geophysics*, 68, 559–565, <https://doi.org/10.1190/1.1567225>, 2003.
- Mott, R., Stiperski, I., and Nicholson, L.: Spatio-temporal flow variations driving heat exchange processes at a mountain glacier, *The Cryosphere*, 14, 4699–4718, <https://doi.org/10.5194/tc-14-4699-2020>, 2020.
- Murray, T., Stuart, G. W., Fry, M., Gamble, N. H., and Crabtree, M. D.: Englacial water distribution in a temperate glacier from surface and borehole radar velocity analysis, *J. Glaciol.*, 46, 389–398, <https://doi.org/10.3189/172756500781833188>, 2000.
- Murray, T., Booth, A., and Rippin, D. M.: Water-Content of Glacier-Ice: Limitations on Estimates from Velocity Analysis of Surface Ground-Penetrating Radar Surveys, *JEEG*, 12, 87–99, <https://doi.org/10.2113/jeeg12.1.87>, 2007.
- Navarro, F. and Eisen, O. (Eds.): 11 Ground-penetrating radar in glaciological applications, in: Remote sensing of glaciers: Techniques for topographic, spatial and thematic mapping of glaciers, CRC Press, 195–229, <https://doi.org/10.1201/b10155-12>, 2009.
- Nobes, D.: The directional dependence of the Ground Penetrating Radar response on the accumulation zones of temperate Alpine glaciers, *First Break*, 17, 249–259, <https://doi.org/10.1046/j.1365-2397.1999.00028.x>, 1999.
- Nobes, D. C. and Annan, A. P.: “Broadside” versus “end-fire” radar response: some simple illustrative examples, Eighth International Conference on Ground Penetrating Radar, 696–701, <https://doi.org/10.1117/12.383501>, 2000.
- Ogier, C., Van Manen, D.-J., Maurer, H., Räss, L., Hertrich, M., Bauder, A., and Farinotti, D.: Ground penetrating radar in temperate ice: englacial water inclusions as limiting factor for data interpretation, *J. Glaciol.*, 1–12, <https://doi.org/10.1017/jog.2023.68>, 2023.
- Pelto, B. M., Maussion, F., Menounos, B., Radić, V., and Zeuner, M.: Bias-corrected estimates of glacier thickness in the Columbia River Basin, Canada, *J. Glaciol.*, 66, 1051–1063, <https://doi.org/10.1017/jog.2020.75>, 2020.
- Raper, S. C. B., Brown, O., and Braithwaite, R. J.: A geometric glacier model for sea-level change calculations, *Journal of Glaciology*, 46, 357–368, <https://doi.org/10.3189/172756500781833034>, 2000.
- Rippin, D. M., Carrivick, J. L., and Williams, C.: Evidence towards a thermal lag in the response of Kårsaglaciären, northern Sweden, to climate change, *J. Glaciol.*, 57, 895–903, <https://doi.org/10.3189/002214311798043672>, 2011.
- Robin, G. D. Q.: Velocity of radio waves in ice by means of a bore-hole interferometric technique, *J. Glaciol.*, 15, 151–159, <https://doi.org/10.3189/S0022143000034341>, 1975.
- Ruols, B., Baron, L., and Irving, J.: Development of a drone-based ground-penetrating radar system for efficient and safe 3D and 4D surveying of alpine glaciers, *J. Glaciol.*, 69, 2087–2098, <https://doi.org/10.1017/jog.2023.83>, 2023.
- Ruols, B., Klahold, J., Farinotti, D., and Irving, J.: 4D GPR imaging of a near-terminus glacier collapse feature, *The Cryosphere*, 19, 4045–4059, <https://doi.org/10.5194/tc-19-4045-2025>, 2025.
- Rutishauser, A., Maurer, H., and Bauder, A.: Helicopter-borne ground-penetrating radar investigations on temperate alpine glaciers: A comparison of different systems and their abilities for bedrock mapping, *GEOPHYSICS*, 81, WA119–WA129, <https://doi.org/10.1190/GEO2015-0144.1>, 2015.



- Santin, I., Colucci, R. R., Žebre, M., Pavan, M., Cagnati, A., and Forte, E.: Recent evolution of Marmolada glacier (Dolomites, Italy) by means of ground and airborne GPR surveys, *Remote Sensing of Environment*, 235, 111442, <https://doi.org/10.1016/j.rse.2019.111442>, 2019.
- Schohn, C. M., Iverson, N. R., Zoet, L. K., Fowler, J. R., and Morgan-Witts, N.: Linear-viscous flow of temperate ice, *Science*, 435, 387, 182–185, <https://doi.org/10.1126/science.adp7708>, 2025.
- Schroeder, D. M., Bingham, R. G., Blankenship, D. D., Christianson, K., Eisen, O., Flowers, G. E., Karlsson, N. B., Koutnik, M. R., Paden, J. D., and Siegert, M. J.: Five decades of radioglaciology, *Ann. Glaciol.*, 61, 1–13, <https://doi.org/10.1017/aog.2020.11>, 2020.
- Sevestre, H., Benn, D. I., Hulton, N. R. J., and Bælum, K.: Thermal structure of Svalbard glaciers and implications for thermal switch models of glacier surging, *J. Geophys. Res. Earth Surf.*, 120, 2220–2236, <https://doi.org/10.1002/2015JF003517>, 2015.
- Stocker-Waldhuber, M., Fischer, A., Helfricht, K., Kuhn, M., Schneider, H., and Span, N.: Glacier surface velocities of Hintereisferner, 2022/2023, <https://doi.org/10.1594/PANGAEA.970134>, 2024.
- Strasser, U., Marke, T., Braun, L., Escher-Vetter, H., Juen, I., Kuhn, M., Maussion, F., Mayer, C., Nicholson, L., Niedertscheider, K., Sailer, R., Stötter, J., Weber, M., and Kaser, G.: The Rofental: a high Alpine research basin (1890–3770 m a.s.l.) in the Ötztal Alps (Austria) with over 150 years of hydrometeorological and glaciological observations, *Earth Syst. Sci. Data*, 10, 151–171, <https://doi.org/10.5194/essd-10-151-2018>, 2018.
- Švinka, L., Karušs, J., and Lamsters, K.: Ice thickness inversion assessment: A comparison study for Waldemarbreen and Irenebreen glaciers, Svalbard, *Polar Science*, 43, 101167, <https://doi.org/10.1016/j.polar.2025.101167>, 2025.
- Švinka, L., Lamsters, K., Karušs, J., Džeriņš, P., Ješkins, J.: Supplementary materials for the publication "GPR-derived ice thickness of the temperate Hintereisferner glacier (Austrian Alps): evaluation of thickness models", Zenodo [data set], <https://doi.org/10.5281/zenodo.18542682>, 2026.
- Tjoelker, A. R., Baraër, M., Valence, E., Charonnat, B., Masse-Dufresne, J., Mark, B. G., and McKenzie, J. M.: Drone-Based Ground-Penetrating Radar with Manual Transects for Improved Field Surveys of Buried Ice, *Remote Sensing*, 16, 2461, <https://doi.org/10.3390/rs16132461>, 2024.
- Voordendag, A., Prinz, R., Schuster, L., and Kaser, G.: Brief communication: The Glacier Loss Day as an indicator of a record-breaking negative glacier mass balance in 2022, *The Cryosphere*, 17, 3661–3665, <https://doi.org/10.5194/tc-17-3661-2023>, 2023a.
- Voordendag, A., Goger, B., Klug, C., Prinz, R., Rutzinger, M., Sauter, T., and Kaser, G.: Uncertainty assessment of a permanent long-range terrestrial laser scanning system for the quantification of snow dynamics on Hintereisferner (Austria), *Front. Earth Sci.*, 11, 1085416, <https://doi.org/10.3389/feart.2023.1085416>, 2023b.
- Watts, R. D. and England, A. W.: Radio-echo Sounding of Temperate Glaciers: Ice Properties and Sounder Design Criteria, *J. Glaciol.*, 17, 39–48, <https://doi.org/10.3189/S0022143000030707>, 1976.
- WGMS: Fluctuations of Glaciers Database, <https://doi.org/10.5904/wgms-fog-2024-01> (last access:10 November 2025), 2024.

<https://doi.org/10.5194/egusphere-2026-783>

Preprint. Discussion started: 5 March 2026

© Author(s) 2026. CC BY 4.0 License.



Zekollari, H., Huss, M., and Farinotti, D.: Modelling the future evolution of glaciers in the European Alps under the EURO-
465 CORDEX RCM ensemble, *The Cryosphere*, 13, 1125–1146, <https://doi.org/10.5194/tc-13-1125-2019>, 2019.

Zekollari, H., Huss, M., Schuster, L., Maussion, F., Rounce, D. R., Aguayo, R., Champollion, N., Compagno, L., Hugonnet, R., Marzeion, B., Mojtabavi, S., and Farinotti, D.: Twenty-first century global glacier evolution under CMIP6 scenarios and the role of glacier-specific observations, *The Cryosphere*, 18, 5045–5066, <https://doi.org/10.5194/tc-18-5045-2024>, 2024.